PAPER

Check for updates

A novel overtone peak self-referencing fluorescent sensor based on a bipyridine-linked covalent organic framework for highly sensitive copper ion detection†

Tongfu Huang, [ID] [a] Wei Xiong,[a] Fusheng Liao,[a] Guobing Wei, [ID] [a] Zhaojiang Yin*[b] and Hao Fan [ID] *[a]

This study reports a novel ratiometric fluorescence sensor based on a tetraphenylethylene-bipyridine covalent organic framework (TPE-Bpy-COF) for the sensitive detection of Cu^{2+}, leveraging the unique coordination properties of the bipyridine moieties. The interaction between Cu^{2+} and the nitrogen atoms in the bipyridine units induces fluorescence quenching at 500 nm through an efficient host–guest electron transfer mechanism, where excited-state electrons from the COF framework are transferred to the vacant orbitals of Cu^{2+}. Upon excitation at 410 nm, the sensor exhibits a primary emission peak at 500 nm, which is quenched in the presence of Cu^{2+}, while an overtone peak at 820 nm remains stable, serving as an internal reference for ratiometric measurements and significantly enhancing the accuracy and reliability of the sensor. The detection limit for Cu^{2+} is 0.1 μM, with the dual-emission system and the strong affinity of the bipyridine units for Cu^{2+}, further improving the sensor's sensitivity and selectivity. Additionally, the sensor demonstrated excellent recovery rates in real water samples, confirming its practical applicability in environmental monitoring.

1. Introduction

Copper is a widely distributed element in nature, crucial for physiological processes in the human body, and is a common environmental heavy metal contaminant.[1–3] It is essential for neurotransmitter regulation,[4] hematopoiesis,[5] cellular metabolism,[6] and the growth of vital organs, including the liver and heart.[7,8] Nevertheless, an excess of copper in the body can trigger the overproduction of reactive oxygen species (ROS), leading to oxidative stress and disrupting normal cellular metabolic processes.[9] Conversely, copper deficiency can cause health issues such as osteoarticular diseases[10] and anemia.[11] According to guidelines from the World Health Organization (WHO) and the Environmental Protection Agency (EPA), the maximum allowable concentrations of copper ions in drinking water are 1.3 mg L^{-1} (20.4 μM) and 2.0 mg L^{-1} (31.4 μM),[12] respectively. Therefore, enhancing the selectivity and sensitivity of copper ion detection in environmental and medical applications is of critical importance.

[a]*Jiangxi University of Chinese Medicine, Nan Chang, Jiangxi 330004, China*
[b]*Clinical Medical Research Center, Yichun People's Hospital, Yichun, Jiangxi 336000, China*
† Electronic supplementary information (ESI) available. See DOI: https://doi.org/10.1039/d4ay01738b

Traditional methods for detecting copper ions, such as flame atomic absorption spectroscopy (AAS) and inductively coupled plasma mass spectrometry (ICP-MS),[13,14] typically involve complex and costly instrumentation, limiting their widespread use. In contrast, fluorescence analysis has been widely employed for detecting copper ion levels in environmental and biological samples due to its high sensitivity, strong selectivity, low detection limits, rapid response, and ease of operation.[15,16] In recent years, various novel nano-fluorescent materials, including polymers,[17,18] nanoparticles,[19,20] quantum dots,[21,22] and organic dyes,[23,24] have been developed for copper detection. Despite advancements in fluorescence sensors for copper ion detection, single-emission methods are easily influenced by factors such as concentration, stability, instrumentation, pH, temperature, and buffer solutions, leading to unstable results or indistinguishable false positives and negatives. By contrast, the overtone peak reference approach uses specific emission peaks to monitor environmental fluctuations, where shifts in the intensity or position of these peaks indicate disturbances in the environment. Monitoring these variations allows for correction of errors from environmental factors, thereby improving analytical accuracy and reliability.[25–27] Consequently, there is a pressing need to develop fluorescence detection methods with multi-emission strategies for targeted detection.

Covalent organic frameworks (COFs) are highly ordered materials formed by the covalent bonding of organic

monomers. Owing to their chemical stability, tunable functionality, large specific surface area, uniform pore structure, and abundant binding sites, COFs have been widely investigated for their potential in ion detection.[28–32] Specifically, innovative COFs with adjustable properties and functional groups show great promise as fluorescent materials for addressing environmental issues related to heavy metal ion contamination. Previous studies have demonstrated that incorporating different luminescent units into COFs can lead to the development of highly efficient luminescent COF sensors.[33–35] Therefore, the organic ligand tetraphenylethylene (TPE), known for its aggregation-induced emission (AIE), is an ideal choice for designing fluorescent COFs.[36,37] The porous structure of COFs creates a favorable microenvironment for the aggregation of TPE molecules, thereby enhancing the AIE effect and fluorescence emission.[38]

Based on the above considerations, we designed a fluorescent covalent organic framework with abundant coordination sites, synthesized by a condensation reaction using tetraphenylethene-4-carboxaldehyde (TPE-CHO) and 5,5′-diamino-2,2′-bipyridine (Bpy) as building units. Under 410 nm excitation, the COF exhibits a overtone peak at 820 nm, which serves as a self-referencing signal to minimize signal deviation due to environmental fluctuations. The bipyridine groups show high affinity for Cu^{2+} ions, and during coordination, Cu^{2+} acts as an electron acceptor, coordinating with the bipyridine groups in the COF and accepting the lone pair electrons from nitrogen atoms. This coordination induces electron transfer from the excited TPE-Bpy-COF to the unfilled 3d orbitals of Cu^{2+}, resulting in fluorescence quenching at 500 nm (Scheme 1). Based on this characteristic, we successfully constructed a fluorescence sensor using the overtone peak as a self-referencing signal, enabling high-sensitivity detection of Cu^{2+} ions in water samples.

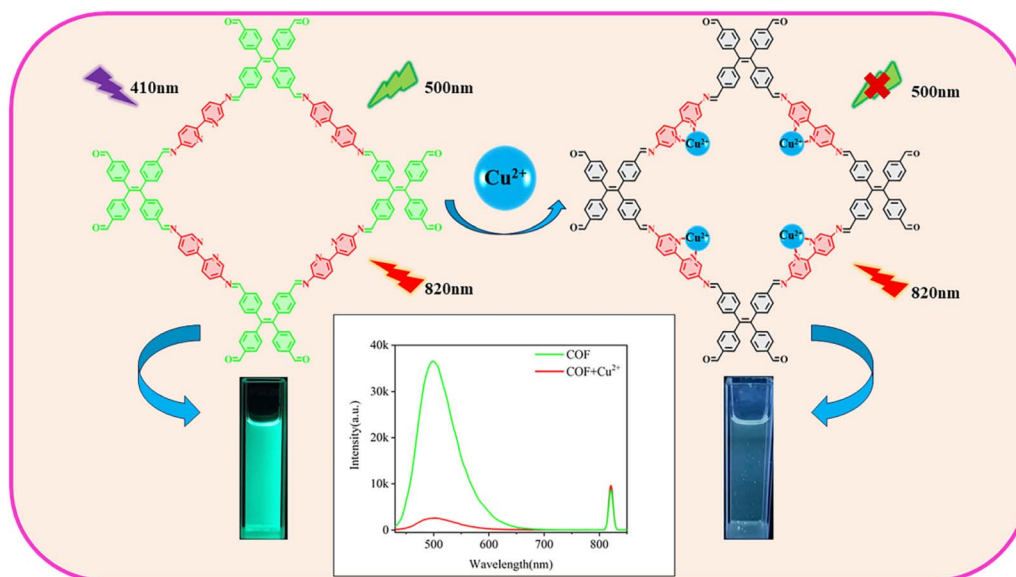# 2. Experimental

2.1. Reagents

Tetra-(4-formylphenyl)ethylene (TPE-CHO) and 5,5′-diamino-2,2′-bipyridine (Bpy) were obtained from Macklin Biochemical Technology Co., Ltd (Shanghai, China). *o*-Dichlorobenzene (*o*-DCB), *N*,*N*-dimethylacetamide (DMAC), glacial acetic acid, and ethylenediaminetetraacetic acid (EDTA) were obtained from Shanghai Aladdin Biochemical Technology Co., Ltd (Shanghai, China). Copper chloride was obtained from Xilong Scientific Co., Ltd (Guangdong, China). All other chemical reagents were of analytical grade and were used without further purification. Ultrapure water (18.2 MΩ cm) was supplied by a Milli-Q system (Millipore).

2.2. Instruments

The morphology of the TPE-Bpy-COF was examined using a LEO-1530VP scanning electron microscope (SEM) from Zeiss, Germany. The Fourier-transform infrared spectra (FT-IR) were recorded using a Bruker VERTEX70 spectrometer (Ettlingen, Germany). X-ray photoelectron spectroscopy (XPS) was performed at 77 K using a Thermo Escalab 250xi photoelectron spectrometer (USA). Fluorescence lifetimes were measured using an Edinburgh Instruments FLS920 system. Emission and excitation spectra were obtained using a Hitachi FL-4500 fluorescence spectrometer. In the fluorescence experiments, the excitation wavelength was set to 410 nm, with slit widths of 5 nm for excitation and 2.5 nm for emission. All fluorescence measurements were conducted under consistent experimental parameters.

2.3. Synthesis of the TPE-Bpy-COF

The TPE-Bpy-COF was synthesized with Bpy and TPE-CHO as its structural components, forming a bipyridine-linked COF through a solvothermal reaction. TPE-CHO (0.05 mmol) was first dissolved

Scheme 1 Schematic diagram of Cu^{2+} detection by the TPE–Bpy–COF sensor.

in a glass vial containing a DMAC/*o*-DCB solvent mixture (0.8 mL, v/v = 3 : 1) using sonication. Subsequently, Bpy (0.1 mmol) was added to the solution, and the mixture was sonicated until fully dissolved. Next, glacial acetic acid (12.0 M, 80 μL) was added, and the vial was vacuum-sealed. The mixture was subsequently heated at 120 °C for 3 days, yielding a yellow precipitate. After cooling to room temperature, the mixture was centrifuged at 10 000 rpm for 10 minutes, and the resulting solid was washed three times with methanol to remove unreacted starting materials and solvents trapped within the pores. The final material was dried at 60 °C for 8 hours, resulting in a light yellow powder.

2.4. Optimization of experimental conditions for the TPE-Bpy-COF

TPE-Bpy-COF suspensions (0.1 mg L^{-1}) were prepared in various solvents, including DMF, DMSO, methanol, ethanol, acetonitrile, water, and water/ethanol mixtures. Following ultrasonic mixing, the fluorescence intensity was measured immediately. To examine the effect of TPE-Bpy-COF concentration on fluorescence intensity, a series of samples with varying concentrations were prepared. Additionally, the pH of a 0.06 mg mL^{-1} suspension was adjusted between 3 and 9 using HCl and NaOH to evaluate its influence on fluorescence intensity.

2.5. Fluorescence detection of Cu^{2+}

The TPE-Bpy-COF (1.2 mg) was dispersed in a 20 mL ethanol/water mixture (8 : 2 v/v) and sonicated for 10 minutes to prepare a 0.06 mg mL^{-1} TPE-Bpy-COF suspension. Two milliliters of this suspension was placed in a quartz cuvette, and Cu^{2+} solutions (0.05–16.0 μM) were incrementally added in 10 μL aliquots, resulting in final Cu^{2+} concentrations ranging from 0 to 8.0 μM. After each addition, the fluorescence spectra were recorded to evaluate the fluorescence response of the TPE-Bpy-COF to Cu^{2+}.

2.6. Preparation of real samples

To evaluate the practical applicability of the proposed sensor, copper ion levels were detected in tap water and river water samples. The river water samples were first centrifuged and filtered using a 0.45 μm syringe filter to remove any insoluble particles. The tap water samples were used without treatment. Different concentrations of Cu^{2+} solution were then added to the processed water samples for the analysis.

3. Results and discussion

3.1. Characterization of the TPE-Bpy-COF

The occurrence of the Schiff base reaction was confirmed through Fourier-transform infrared spectroscopy (FT-IR). As shown in Fig. 1A, a characteristic band at 1627 cm^{-1} corresponding to the stretching vibration of the C=N bond was observed, indicating a successful Schiff base reaction between the monomers.[39,40] Furthermore, the absorption peaks at 3416 cm^{-1} and 3330 cm^{-1} are associated with the amino groups of 2,2′-bipyridine-5,5′-diamine, while the characteristic peak at
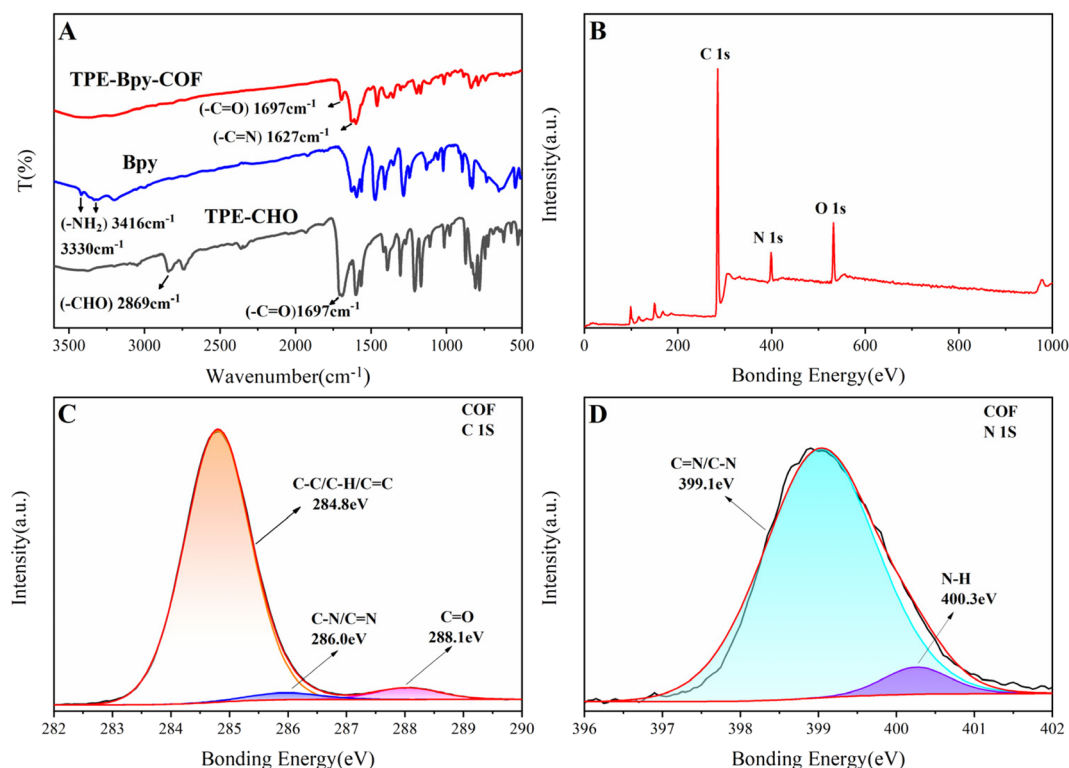

Fig. 1 (A) FT-IR spectral images of tetra-(4-formylphenyl)ethylene, 5,5′-diamino-2,2′-bipyridine, and the TPE-Bpy-COF. (B) XPS spectra of the TPE-Bpy-COF. (C) C 1s, (D) N 1s.
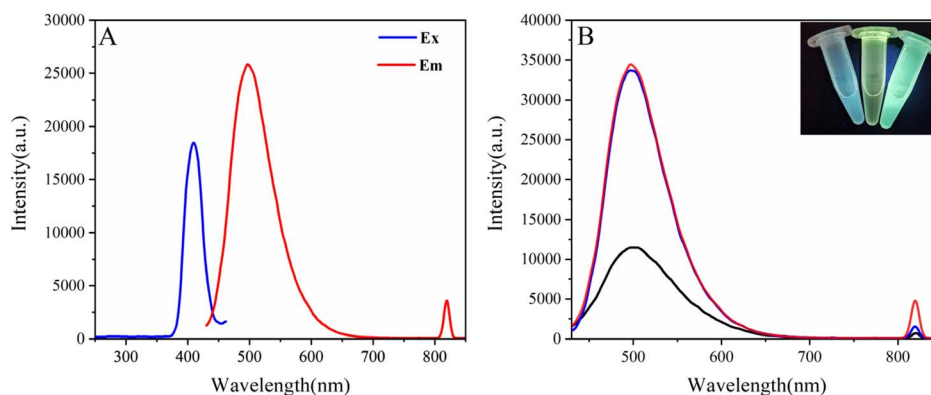
Fig. 2 (A) λ_{Ex} = 410 nm for the TPE-Bpy-COF, the fluorescence emission spectra are λ_{Em} = 500 nm and λ_{Em} = 820 nm. (B) Fluorescence emission spectra of TPE-CHO (black line), Bpy (blue line), and the TPE-Bpy-COF (red line). The upper right side of the image is the luminescent image of the sample, from left to right, Bpy, TPE-CHO and the TPE-Bpy-COF.

1697 cm^{-1} is attributed to the aldehyde groups of tetra-(4-for-mylphenyl)ethylene. The peaks at 3062 cm^{-1} and 2862 cm^{-1} correspond to the stretching vibrations of unsaturated –CH groups.[39] The disappearance of the peaks for Bpy (–NH$_2$ at 3282 cm^{-1}) and TPE-CHO (–CHO at 2896 cm^{-1}), along with a significant reduction in the absorption intensity of –C=O at 1697 cm^{-1} in the FT-IR spectrum, further confirms the successful formation of the COF.

X-ray photoelectron spectroscopy (XPS) was utilized to analyze the chemical composition and surface electronic states of the TPE-Bpy-COF. The presence of C 1s, N 1s, and O 1s was indicated by peaks at 284.4, 399.1, and 531.4 eV, respectively (Fig. 1B). The high-resolution C 1s spectrum revealed peaks at 284.8 eV, 286 eV, and 288.1 eV, corresponding to C–C/C–H in aromatic rings, C–N/C=N, and aldehyde C=O groups (Fig. 1C).[39] N 1s peaks at 399.1 eV and 400.3 eV indicated the presence of –C=N, pyridinic nitrogen, and free secondary amines (–NH) (Fig. 1D).[41] The appearance of –C=N confirms the formation of imine bonds, verifying the successful synthesis of the TPE-Bpy-COF. Moreover, SEM images of the TPE-Bpy-COF (Fig. S1A†) showed a rough surface featuring nanosheets and aggregated structures. Elemental mapping (Fig. S1B–D†) further reveals that carbon, nitrogen, and oxygen are evenly distributed throughout the framework.

The fluorescence spectra of the TPE-Bpy-COF were recorded, revealing strong emission at 500 nm under 410 nm excitation (Fig. 2A). Comparative spectra showed that the TPE-Bpy-COF exhibited significantly higher fluorescence intensities at 500 nm and 820 nm compared to the tetra-(4-formylphenyl) ethylene monomer (Fig. 2B), confirming that the AIE effect within the TPE-Bpy-COF's porous framework enhances fluorescence emission.

3.2. Optimization of the experimental conditions

The fluorescence emission spectra of the TPE-Bpy-COF in various solvents are presented in Fig. 3A. Compared to dispersion in DMF, methanol, ethanol, acetonitrile, and water, the TPE-Bpy-COF exhibited higher fluorescence intensity when dispersed in DMSO and the water/ethanol mixed solvent. Considering the high toxicity of DMSO, its practical application is limited. In contrast, the water–ethanol mixed solvent provides moderate aggregation, prevents excessive aggregation, and enhances the AIE effect. Therefore, the water–ethanol mixed solvent was selected for subsequent experiments. The fluorescence intensity reached its maximum when the TPE-Bpy-COF concentration was 0.06 mg mL^{-1} (Fig. 3B). As the concentration increased further, the intensity of the fluorescence emission peak slightly decreased. Therefore, 0.06 mg mL^{-1} was selected as the optimal concentration of the TPE-Bpy-COF for subsequent experiments. In addition, the effect of pH on the fluorescence intensity of the TPE-Bpy-COF was examined over a pH range of 3 to 9 (Fig. 3C). Under acidic conditions, the
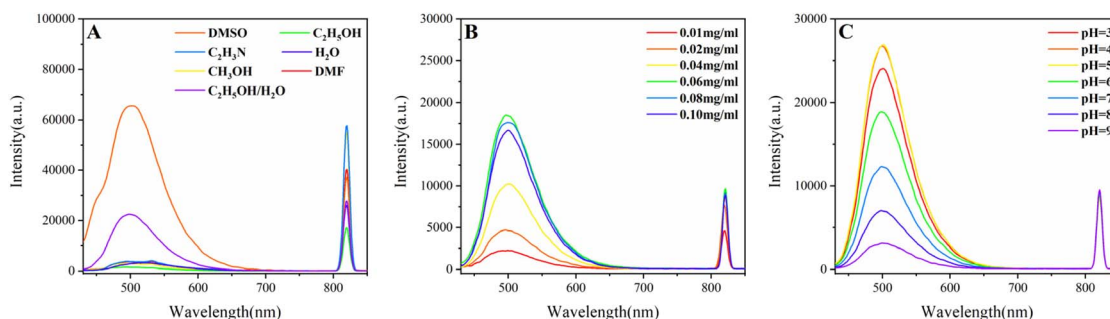

Fig. 3 (A) Fluorescence emission spectrum of the TPE-Bpy-COF in different solvents. (B) The plot of fluorescence intensity versus TPE-Bpy-COF concentration. (C) TPE-Bpy-COF fluorescence emission spectra at different pH values.
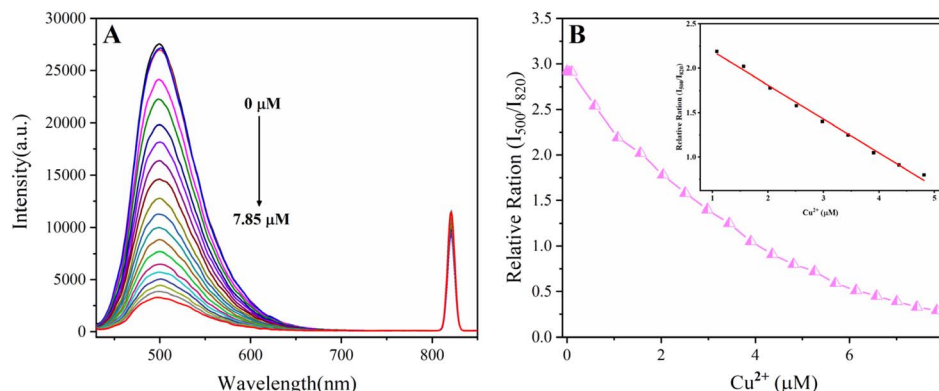
Fig. 4 (A) Fluorescence spectrum of the TPE-Bpy-COF at different Cu^{2+} concentrations. (B) Diagram of the fluorescence intensity at 500 nm and 820 nm *versus* Cu^{2+} concentration (0–7.85 μM). Inset: Linearity of Cu^{2+} concentration (1–5.0 μM) and fluorescence intensity ratio (I_{500}/I_{820}).

nitrogen atoms in the pyridine rings of the TPE-Bpy-COF are protonated to form pyridinium groups, which leads to a redistribution of the electronic structure and makes the charge transfer transition more efficient. Protonation also reduces the LUMO–HOMO energy gap, thus lowering the energy required for the transition and making fluorescence more easily excitable.[42] Notably, at pH = 5, the fluorescence intensity reaches its maximum. Under overly acidic or basic conditions, excessive protonation or deprotonation enhances intermolecular repulsion, affects the stability of the electronic structure, and increases non-radiative energy dissipation, thereby reducing fluorescence. Therefore, pH = 5 was selected as the condition for metal ion sensing to achieve the optimal fluorescence response.

3.3. Quantitative determination of the Cu^{2+} ions

To assess the sensing capabilities of the TPE-Bpy-COF for Cu^{2+}, various concentrations of Cu^{2+} solution were gradually added to the TPE-Bpy-COF suspension, and the fluorescence emission spectra of the resulting mixtures were recorded at 500 nm and 820 nm upon excitation at 410 nm. The emissions at both 500 nm and 820 nm were utilized to quantify the concentration of Cu^{2+}. Notably, the emission at 820 nm remained stable even

with the addition of varying concentrations of Cu^{2+}. As a result, the overtone peak at 820 nm was employed as a self-referencing signal to minimize interference, ensuring the consistency of results across parallel samples and mitigating the effects of temperature and concentration variations.[43] As illustrated in Fig. 4A, the fluorescence quenching effect became more pronounced with increasing concentrations of copper ions, with approximately 90% of the initial COF fluorescence intensity quenched at a Cu^{2+} concentration of 7.85 μM. Fig. 4B shows that the fluorescence intensity ratio of the TPE-Bpy-COF at 500 nm and 820 nm decreases as the Cu^{2+} concentration increases. The linear relationship between the fluorescence intensity ratio and Cu^{2+} concentration is shown in Fig. 5B, exhibiting good linearity within the range of 1.0–4.8 μM, with a detection limit (3σ) of 0.1 μM. The regression equation is $I_{500}/I_{820} = 2.57452 - 0.38179C$, with $R^2 = 0.99378$.

To further assess the detection capability of the TPE-Bpy-COF, the detection limits of various Cu^{2+} fluorescent probes reported in the literature are summarized in Table 1. The TPE-Bpy-COF sensor demonstrates superior detection performance compared to most single-emission and multiple-emission fluorescent probes. As one of the few ratiometric fluorescent sensors based on COF materials, it exhibits enhanced anti-
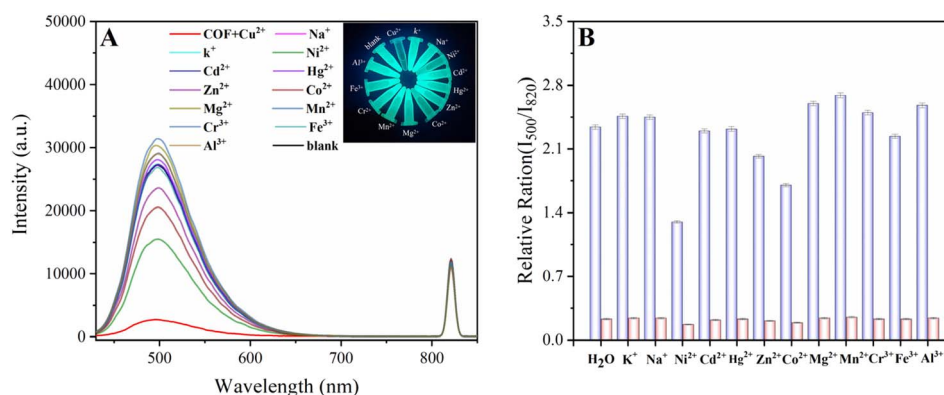

Fig. 5 (A) Selectivity of the TPE-Bpy-COF sensor for Cu^{2+}. (B) Fluorescence intensity ratio (I_{500}/I_{820}) of the TPE-Bpy-COF sensor in the presence of various interfering substances.

Table 1 Comparison with other previously reported Cu^{2+} fluorescent sensors

Fluorescent probes	Methods	Linear range (μM)	LOD (μM)	Ref.
TFPB-DHzDs COF	Fluorescence	0.1–5.0	47.8	44
Sugar and rhodamine based probe	Fluorescence	0.5–4	10	45
Shiff base containing ferrocenyl-1,3,4-thiadiazole	Fluorescence	2–4.8	0.44	46
Sulfur quantum dots	Fluorescence	20–200	6.78	47
ZnSe quantum dots	Fluorescence	0–6	0.47	48
AuNCs/PQD@SiO$_2$	Ratio fluorescence	0–160	3	49
PTA-NH$_2$@GSH-AuNCs	Ratio fluorescence	1–150	0.275	50
NCs/QDs	Ratio fluorescence	0.3–3	0.12	51
TPE-Bpy-COF	Ratio fluorescence	1.0–4.8	0.1	This work

interference capabilities, further improving the reliability and precision of detection.

3.4. Selectivity assessment of the sensor for Cu^{2+}

To validate the practical applicability of the TPE-Bpy-COF for Cu^{2+} detection, its selectivity and interference resistance were systematically evaluated. The TPE-Bpy-COF was dispersed in an ethanol/water mixture, and equal amounts of various metal salt solutions were added to form suspensions for fluorescence analysis. As illustrated in Fig. 5A, the transition metal ions Zn^{2+}, Co^{2+}, and Ni^{2+} caused only minor quenching of fluorescence emission at 500 nm, while other metal ions such as Na^+, K^+, Mg^{2+}, Ca^{2+}, Mn^{2+}, Cd^{2+}, Hg^{2+}, Al^{3+}, and Fe^{3+} had a negligible impact on TPE-Bpy-COF's fluorescence intensity. Among all the metal ions tested, Cu^{2+} demonstrated the most significant fluorescence quenching response. Additionally, the selectivity of the TPE-Bpy-COF for Cu^{2+} was further tested in the presence of potential interfering ions. These interference tests involved mixing the COF suspension containing 10 μM Cu^{2+} with other metal ions at a concentration of 50 μM each. Fig. 5B shows that under optimal experimental conditions, the presence of these interfering ions had minimal impact on Cu^{2+} detection by the TPE-Bpy-COF, confirming its high selectivity and strong anti-interference capability. Consequently, the TPE-Bpy-COF sensing platform is effective for the selective and sensitive detection of copper ions.

3.5. Stability and regeneration performance of the sensor for Cu^{2+}

The optical stability and regeneration properties of the TPE-DPE-COF sensor were evaluated. The optical stability of the sensor in ethanol/water (8 : 2 v/v) was investigated by measuring the fluorescence intensity over time at room temperature. As shown in Fig. S2A,† intermittent fluorescence emission was measured for 168 h, and the peak intensity remained stable. The TPE-Bpy-COF was regenerated by adding a strong chelating agent (EDTA) to the COF suspension containing copper ions. As depicted in Fig. S2B,† the fluorescence intensity of the TPE-Bpy-COF nearly returned to its initial level after EDTA regeneration. The results showed that the TPE-Bpy-COF maintained its original fluorescence intensity even after three cycles, demonstrating excellent regeneration properties.

3.6. Quenching mechanism

The interaction mechanism between the TPE-Bpy-COF and Cu^{2+} ions was investigated using time-resolved fluorescence spectroscopy to examine the quenching effect of Cu^{2+} on the TPE-Bpy-COF. The fluorescence lifetime of the COF decreased markedly from 2.89 ns to 1.04 ns upon Cu^{2+} addition (Fig. 6A and Table S1†), indicating that the quenching mechanism likely involves electron transfer or fluorescence resonance energy transfer (FRET).[52] For FRET to occur, the excitation spectrum of the sensor must overlap with the UV-visible absorption
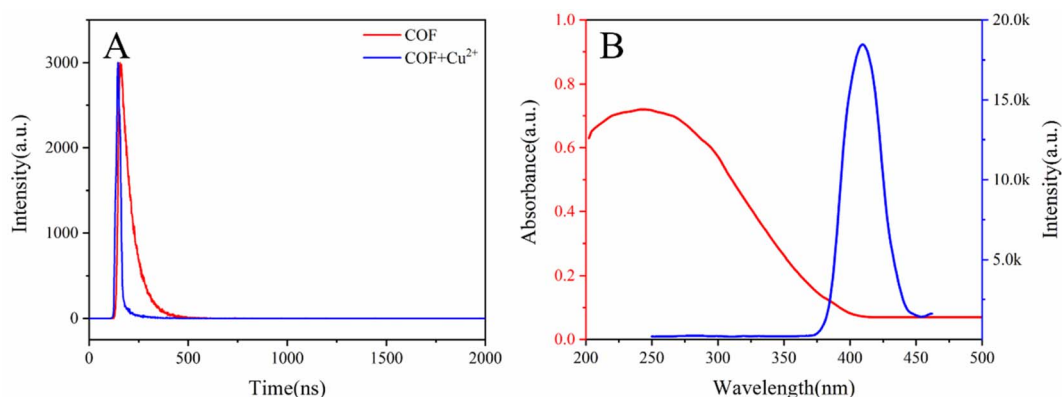

Fig. 6 (A) Fluorescence lifetime (500 nm) of the TPE-Bpy-COF sensor in the absence of Cu^{2+}/presence of Cu^{2+}. (B) UV absorption spectra of Cu^{2+} (red line) and excitation spectrum of the TPE-Bpy-COF sensor (blue line).
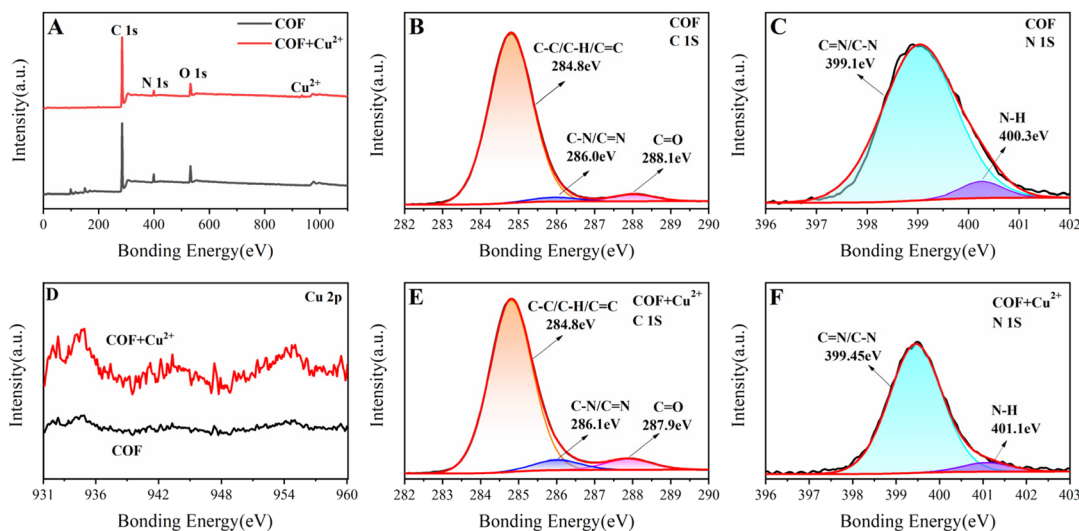
Fig. 7 (A) XPS spectra of the COF and COF loaded with Cu^{2+}. (B) C 1s XPS spectra of the COF. (C) N 1s XPS spectra of the COF. (D) Cu 2p XPS spectra of the COF and the COF loaded with Cu^{2+}. (E) C 1s XPS spectra of the COF loaded with Cu^{2+}. (F) N 1s XPS spectra of the COF loaded with Cu^{2+}.

spectrum of the analyte. However, as shown in Fig. 6B, there is no overlap between the excitation spectrum of the TPE-Bpy-COF and the UV-visible absorption of copper ions, effectively ruling out FRET as the quenching mechanism.

Based on the above discussion, it is proposed that the fluorescence quenching is primarily caused by the host–guest electron transfer between Cu^{2+} and the TPE-Dpy-COF. In this process, Cu^{2+} acts as an electron acceptor, coordinating with the pyridine groups in the TPE-Dpy-COF and accepting lone pair electrons from nitrogen atoms. This interaction facilitates the transfer of excited-state electrons from the TPE-Dpy-COF to the unfilled 3d orbitals of Cu^{2+}, resulting in fluorescence quenching at 500 nm. The X-ray photoelectron spectroscopy (XPS) analysis of the TPE-Dpy-COF and TPE-Dpy-COF@Cu confirms the coordination between Cu^{2+} ions and the bipyridine groups, with the structural characterization showing that the presence of Cu^{2+} is evident in the XPS survey spectrum (Fig. 7A) and the Cu 2p spectrum (Fig. 7D). The signals at 936.5 eV and 956.7 eV correspond to Cu $2p_{3/2}$ and Cu $2p_{1/2}$ respectively,[53] indicating successful binding of Cu^{2+} with the TPE-Bpy-COF. Comparing the C 1s spectra (Fig. 7B and E) before and after Cu^{2+} binding reveals a shift of 0.15 eV at 287.9 eV (C=N), attributed to changes in the electron cloud density of carbon atoms during the binding process. The N 1s peaks at 399.1 eV and 400.3 eV (Fig. 7C and F) correspond to pyridinic nitrogen (in imine and bipyridine) and amine nitrogen, respectively. After the addition of Cu^{2+}, the N 1s peak at 399.1 eV in the XPS spectrum (attributed to the C=N bond in the 2,2′-bipyridine group) shifted by 0.35 eV towards higher binding energy. This shift indicates that, due to the coordination between the nitrogen atoms in the bipyridine group and Cu^{2+}, electrons are transferred from the nitrogen atoms to Cu^{2+}, resulting in a decreased electron density around the nitrogen atoms.[54,55]

The selectivity of the COF for Cu^{2+} is due to the unsaturated electron state of the Cu^{2+}'s outer shell (d^9), which makes the

vacant orbitals ideal electron acceptors, thereby more effectively accepting electrons from the nitrogen atoms. The fully filled d^{10} configuration of Zn^{2+} lacks vacant orbitals to accept electrons, making it less likely to participate in electron transfer. In comparison, Co^{2+} and Ni^{2+}, with d^7 and d^8 configurations, may accept electrons under certain conditions, but their electronic structure and lower coordination affinity limit them from achieving the same effect as Cu^{2+} ions.[56,57] The slight fluorescence quenching caused by transition metal ions Zn^{2+}, Co^{2+}, and Ni^{2+} further supports this explanation.

3.7. Detection of Cu^{2+} in water samples

To evaluate the feasibility and reliability of the TPE-Bpy-COF ratiometric fluorescence sensor for Cu^{2+} detection, the sensor was tested in river and tap water samples with varying concentrations of Cu^{2+} to validate its effectiveness in real water samples. As presented in Table 2, the recovery rates for Cu^{2+} detection ranged from 99.2% to 103.3%, with RSDs of less than 4.0%. The results confirm that the TPE-Bpy-COF ratiometric fluorescence sensor is highly effective for detecting Cu^{2+} in environmental samples, demonstrating its practicality and

Table 2 Detection of Cu^{2+} ions in practical samples ($n = 3$)

Samples	Add (μM)	Found (μM)	Recovery (%)	RSD (%)
River water	0	0.16	—	—
	1	1.17	101.2	4.1
	2	2.14	99.2	1.2
	4	4.18	100.5	1.9
Tap water	0	0	—	—
	1	1.03	103.3	2.1
	2	2.03	101.3	2.4
	4	4.00	100.1	2.6

effectiveness for environmental monitoring and water quality analysis.

4. Conclusion

In conclusion, this research developed a ratiometric fluorescent sensor founded on a TPE-Bpy-COF, incorporating an AIE-active ligand alongside bipyridine units to construct a framework with abundant coordination sites. Upon excitation at 410 nm, this COF displays emissions at both 500 nm and 820 nm. By employing the 820 nm overtone peak as a self-referencing signal, environmental interference was effectively minimized, enabling precise detection of Cu^{2+}. Acting as an electron acceptor, Cu^{2+} binds strongly to the bipyridine moieties in the TPE-Bpy-COF, which in turn causes fluorescence quenching at 500 nm. This sensor reached a detection limit of 0.1 μM, maintaining a linear response from 1.0 to 4.8 μM, and showed high recovery rates in tests with real water samples. This study provides a novel approach for COF-based ratiometric fluorescence detection, showing significant potential for heavy metal ion detection in complex environments.

Data availability

The data supporting this article have been included as part of the ESI.†

Author contributions

Tongfu Huang: writing – original draft, data curation, writing – review & editing; Wei Xiong: methodology, conceptualization; Guobing Wei: funding acquisition, data curation; Fusheng Liao: investigation, data curation; Zhaojiang Yin: supervision; Hao Fan: funding acquisition, resources, methodology, project administration, supervision, writing – review & editing.

Conflicts of interest

The authors declare that they have no known competing financial interests or personal relationships that could have appeared to influence the work reported in this paper.

Acknowledgements

References

1 X. Tian, Y. Zhao, Y. Li, C. Yang and Z. Zhou, *Sens. Actuators, B*, 2017, **247**, 139–145.
2 B.-E. Kim, T. Nevitt and D. J. Thiele, *Nat. Chem. Biol.*, 2008, **4**, 176–185.
3 R. Uauy, M. Olivares and M. Gonzalez, *Am. J. Clin. Nutr.*, 1998, **67**, 952S–959S.
4 R. E. Cowley, L. Tian and E. I. Solomon, *Proc. Natl. Acad. Sci. U. S. A.*, 2016, **113**, 12035–12040.
5 A. Langston, J. Neely, L. Heffner, D. Griffith, M. Arellano, G. Esper, M. L. McLemore, T. Ziegler, C. Kempton and R. Sinha, *Blood*, 2008, **112**, 3094.
6 W. Wang, W. Mo, Z. Hang, Y. Huang, H. Yi, Z. Sun and A. Lei, *ACS Nano*, 2023, **17**, 19581–19599.
7 E. L. Que, D. W. Domaille and C. J. Chang, *Chem. Rev.*, 2008, **108**, 1517–1549.
8 Z. Wu, G. Lv, F. Xing, W. Xiang, Y. Ma, Q. Feng, W. Yang and H. Wang, *Cancer Lett.*, 2023, 216348.
9 S. C. Dodani, A. Firl, J. Chan, C. I. Nam, A. T. Aron, C. S. Onak, K. M. Ramos-Torres, J. Paek, C. M. Webster and M. B. Feller, *Proc. Natl. Acad. Sci. U. S. A.*, 2014, **111**, 16280–16285.
10 J. Han, J. Luo, C. Wang, L. Kapilevich and X.-a. Zhang, *Biomed. Pharmacother.*, 2024, **174**, 116570.
11 P. Sharp, *Proc. Nutr. Soc.*, 2004, **63**, 563–569.
12 Y. Si, Y. Li, J. Guo, H. Wang, X. Wang and J. Fu, *Talanta*, 2024, **273**, 125941.
13 E. H. Evans, J. A. Day, C. D. Palmer, W. J. Price, C. M. Smith and J. F. Tyson, *J. Anal. At. Spectrom.*, 2005, **20**, 562–590.
14 G. Xing, M. R. Sardar, B. Lin and J.-M. Lin, *Talanta*, 2019, **204**, 50–56.
15 Z. Dong, Y. Yang, X. Cai, X. Tang, Y. Yan, S. Zheng, W. Zhang, S. Cai and J. Fan, *J. Solid State Chem.*, 2022, **316**, 123644.
16 H. Zhang, L. Feng, Y. Jiang, Y.-T. Wong, Y. He, G. Zheng, J. He, Y. Tan, H. Sun and D. Ho, *Biosens. Bioelectron.*, 2017, **94**, 24–29.
17 S. G. Liu, N. Li, Y. Z. Fan, N. B. Li and H. Q. Luo, *Sens. Actuators, B*, 2017, **243**, 634–641.
18 R. Chen, J. You, Y. Chen, Z. Zhang, A. Sun, H. Liu and X. Shi, *Sens. Actuators, B*, 2024, **404**, 135245.
19 G. Abramo and C. A. D'Angelo, *Journal of Informetrics*, 2018, **12**, 249–258.
20 Y. Zhang, S. Xu, X. Li, J. Zhang, J. Sun, L. Tong, H. Zhong, H. Xia, R. Hua and B. Chen, *Sens. Actuators, B*, 2018, **257**, 829–838.
21 T. Han, H. Kang, S. Ye, Y. Yuan, Y. Zhang and L. Dong, *Sci. Total Environ.*, 2020, **746**, 141412.
22 X. Qian, Z. Wang, Z. Chen, S. M. El-Bahy, D. Li, L. Qin, C. Li, Z. M. El-Bahy and J. Zhao, *Colloids Surf., A*, 2024, **693**, 134089.
23 K. Wang, Q. Kong, X. Chen, J. Yoon, K. Swamy and F. Wang, *Chin. Chem. Lett.*, 2020, **31**, 1087–1090.
24 H. Wang, D.-L. Shi, J. Li, H.-Y. Tang, J. Li and Y. Guo, *Sens. Actuators, B*, 2018, **256**, 600–608.

25 W. Ma, Z. Gu, C. Wang, L. Dong, Z. Liu, L. Liu, B. Xu and W. Tian, *CrystEngComm*, 2023, **25**, 3598–3603.

26 C. Cui, Q. Wang, C. Xin, Q. Liu, X. Deng, T. Liu, X. Xu and X. Zhang, *Microporous Mesoporous Mater.*, 2020, **299**, 110122.

27 L. Qin, Q. Yu, Y. Huang, L. Zhang, X. Yan, W. Wu, F. Liao, J. Zhang, H. Cui and J. Zhang, *Anal. Chim. Acta*, 2024, **1287**, 342086.

28 Y. Zhao, Y. Yan, Z. Wu, C. Li, R. Fan, L. Feng, W. Wang and Q. Chen, *J. Mater. Sci.*, 2022, **57**, 13425–13432.

29 Y. Jiang, C. Liu and A. Huang, *ACS Appl. Mater. Interfaces*, 2019, **11**, 32186–32191.

30 Y. Yin and G. Liu, *Anal. Methods*, 2022, **14**, 1988–1995.

31 L. Hou, Y. Jiang, L.-Z. Chen, S.-F. Zhang, H.-Y. Li, M.-J. Wei, F.-Y. Kong and W. Wang, *Anal. Methods*, 2024.

32 H. Hu, Z. Yin, H. Cui, W. Xiong, F. Yu, J. Zhang, F. Liao, G. Wei, L. Yang and J. Zhang, *Anal. Chim. Acta*, 2024, **1330**, 343283.

33 Y. Yan, T. Xia, Y. Zhao, H. Sun, C. Li, R. Fan, W. Wang and Q. Chen, *Mater. Lett.*, 2022, **315**, 131951.

34 G. Lin, H. Ding, D. Yuan, B. Wang and C. Wang, *J. Am. Chem. Soc.*, 2016, **138**, 3302–3305.

35 L. Zhang, F. Guo, S. Xu, Q. Deng, M. Xie, J. Sun, R. T. Kwok, J. W. Lam, H. Deng and H. Jiang, *Adv. Mater.*, 2023, 2304620.

36 S. Wu, H. Min, W. Shi and P. Cheng, *Adv. Mater.*, 2020, **32**, 1805871.

37 P. Jin, C. Guo, J. Li, D. Zhou, G. Xu and Y. Peng, *ACS Appl. Polym. Mater.*, 2023, **5**, 3762–3767.

38 S. Dalapati, E. Jin, M. Addicoat, T. Heine and D. Jiang, *J. Am. Chem. Soc.*, 2016, **138**, 5797–5800.

39 Y. Chen, R. Sun, W. Zhu, Z. Zhang, Y. Chen, S. Wang and Q. Deng, *Sens. Actuators, B*, 2021, **344**, 130216.

40 J. Xiu, N. Zhang, C. Li, A. Salah and G. Wang, *Microporous Mesoporous Mater.*, 2021, **316**, 110979.

41 S.-Y. Li, S. Meng, X. Zou, M. El-Roz, I. Telegeev, O. Thili, T. X. Liu and G. Zhu, *Microporous Mesoporous Mater.*, 2019, **285**, 195–201.

42 R. Bu, L. Zhang, X.-Y. Liu, S.-L. Yang, G. Li and E.-Q. Gao, *ACS Appl. Mater. Interfaces*, 2021, **13**, 26431–26440.

43 S. Asgari, L. Sun, J. Lin, Z. Weng, G. Wu, Y. Zhang and M. Lin, *Microchim. Acta*, 2020, **187**.

44 X. Wu, Y. Zhang, F. Wang, W. Lv, G. Wang, Y. Chen and X. Chen, *Opt. Mater.*, 2023, **140**, 113873.

45 J. Yin, X. Ma, G. Wei, D. Wei and Y. Du, *Sens. Actuators, B*, 2013, **177**, 213–217.

46 H. Ye, F. Ge, Y.-M. Zhou, J.-T. Liu and B.-X. Zhao, *Spectrochim. Acta, Part A*, 2013, **112**, 132–138.

47 A. Huang, X. Yang, T. Xia, D. He, R. Zhang, Z. Li, S. Yang, Y. Liu and X. Wen, *Microchem. J.*, 2022, **179**, 107639.

48 D. Wu, Z. Chen, G. Huang and X. Liu, *Sens. Actuators, A*, 2014, **205**, 72–78.

49 W. Xue, J. Zhong, H. Wu, J. Zhang and Y. Chi, *Analyst*, 2021, **146**, 7545–7553.

50 X. Sun, R. Wen, R. Zhang, Y. Guo, H. Li and Y.-I. Lee, *Microchem. J.*, 2022, **182**, 107877.

51 Z. Wang, R. Liu, Z. Fu, X. Yi, Y. Hu, C. Liu, D. Pan and Z. Wu, *Anal. Methods*, 2023, **15**, 2505–2511.

52 T. Wang, X. Wei, Y. Zong, S. Zhang and W. Guan, *J. Mater. Chem. C*, 2020, **8**, 12196–12203.

53 J. Qi, X. He and Q. Lu, *Chem. Eng. J.*, 2022, **450**, 138203.

54 J. Chen, X. Tao, C. Li, Y. Ma, L. Tao, D. Zheng, J. Zhu, H. Li, R. Li and Q. Yang, *Appl. Catal., B*, 2020, **262**, 118271.

55 C. Liu and B. Yan, *Sens. Actuators, B*, 2016, **235**, 541–546.

56 S. Mandal, R. N. Samajdar, S. Parida, S. Mishra and A. J. Bhattacharyya, *ACS Appl. Mater. Interfaces*, 2022, **14**, 26714–26723.

57 N. W. Kinzel, D. Demirbas, E. Bill, T. Weyhermüller, C. Werlé, N. Kaeffer and W. Leitner, *Inorg. Chem.*, 2021, **60**, 19062–19078.